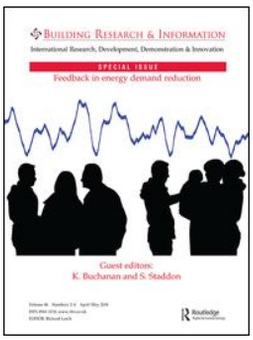

Building Research & Information

ISSN: 0961-3218 (Print) 1466-4321 (Online) Journal homepage: http://www.tandfonline.com/loi/rbri20

Natural ventilation in cities: the implications of fluid mechanics

Jiyun Song, S. Fan, W. Lin, L. Mottet, H. Woodward, M. Davies Wykes, R. Arcucci, D. Xiao, J.-E. Debay, H. ApSimon, E. Aristodemou, D. Birch, M. Carpentieri, F. Fang, M. Herzog, G. R. Hunt, R. L. Jones, C. Pain, D. Pavlidis, A. G. Robins, C. A. Short & P. F. Linden

To cite this article: Jiyun Song, S. Fan, W. Lin, L. Mottet, H. Woodward, M. Davies Wykes, R. Arcucci, D. Xiao, J.-E. Debay, H. ApSimon, E. Aristodemou, D. Birch, M. Carpentieri, F. Fang, M. Herzog, G. R. Hunt, R. L. Jones, C. Pain, D. Pavlidis, A. G. Robins, C. A. Short & P. F. Linden (2018): Natural ventilation in cities: the implications of fluid mechanics, Building Research & Information, DOI: 10.1080/09613218.2018.1468158

To link to this article: https://doi.org/10.1080/09613218.2018.1468158

BUILDING RESEARCH & INFORMATION
2018
https://doi.org/10.1080/09613218.2018.1468158

RESEARCH PAPER

Natural ventilation in cities: the implications of fluid mechanics

Jiyun Song [a,j], S. Fan[b], W. Lin [c], L. Mottet [d,j], H. Woodward[e], M. Davies Wykes [a], R. Arcucci [f], D. Xiao [d], J.-E. Debay[a], H. ApSimon[e], E. Aristodemou[g], D. Birch[c], M. Carpentieri[c], F. Fang[d], M. Herzog[h], G. R. Hunt[i], R. L. Jones[b], C. Pain[d], D. Pavlidis[d], A. G. Robins[c], C. A. Short[j] and P. F. Linden [a]

[a]Department of Applied Mathematics and Theoretical Physics, Centre for Mathematical Sciences, University of Cambridge, Cambridge, UK; [b]Department of Chemistry, University of Cambridge, Cambridge, UK; [c]Department of Mechanical Engineering Sciences, University of Surrey, Guildford, UK; [d]Department of Earth Science and Engineering, Imperial College London, London, UK; [e]Centre for Environmental Policy, Imperial College London, London, UK; [f]Department of Computing, Imperial College, London, UK; [g]School of Engineering, London South Bank University, London, UK; [h]Department of Geography, University of Cambridge, Cambridge, UK; [i]Department of Engineering, University of Cambridge, Cambridge, UK; [j]Department of Architecture, University of Cambridge, Cambridge, UK

ABSTRACT

Research under the Managing Air for Green Inner Cities (MAGIC) project uses measurements and modelling to investigate the connections between external and internal conditions: the impact of urban airflow on the natural ventilation of a building. The test site was chosen so that under different environmental conditions the levels of external pollutants entering the building, from either a polluted road or a relatively clean courtyard, would be significantly different. Measurements included temperature, relative humidity, local wind and solar radiation, together with levels of carbon monoxide (CO) and carbon dioxide (CO_2) both inside and outside the building to assess the indoor–outdoor exchange flows. Building ventilation took place through windows on two sides, allowing for single-sided and crosswind-driven ventilation, and also stack-driven ventilation in low wind conditions. The external flow around the test site was modelled in an urban boundary layer in a wind tunnel. The wind tunnel results were incorporated in a large-eddy-simulation model, Fluidity, and the results compared with monitoring data taken both within the building and from the surrounding area. In particular, the effects of street layout and associated street canyons, of roof geometry and the wakes of nearby tall buildings were examined.

KEYWORDS

air pollutants; air quality; buildings; dispersion; microclimates; modelling; natural ventilation; urban design

Introduction

The global urban population first exceeded the global rural population in 2007 and is expected to reach 6.3 billion in 2050 (United Nations, 2014). During this period of rapid urbanization, change in land use and intensive human activities have led to urban environmental problems, such as the urban heat island, air pollution and excessive energy consumption with associated greenhouse gas (GHG) emissions (Grimmond, 2007). Cities are typically warmer than surrounding rural areas (the heat island) due to higher building densities, the larger thermal mass of construction materials, less vegetation cover and associated radiative processes, and modified wind flow (Oke, 1973; Wilby, 2003). In addition, extreme temperatures associated with heatwaves bring increased health risks to urban populations (Baniassadi & Sailor, 2018; Grimmond, 2007). Urban areas are also major carbon sources, producing approximately 70% of anthropogenic carbon emissions from human respiration and fossil fuel consumption (from industries, transportation *etc.*; UN-Habitat, 2011). Global warming and deteriorating outdoor air quality, accompanied by increased expectations for the quality of indoor environments, result in an increasing energy demand in buildings for cooling using air-conditioning (Sailor, 2001; Sailor & Pavlova, 2003; Santamouris et al., 2001; Santamouris, Cartalis, Synnefa, & Kolokotsa, 2015). This leads to a vicious cycle of increased urban emissions of heat, pollutants and GHGs and an associated increase in energy demand. On the other hand, natural ventilation of buildings provides a sustainable way to cool the indoor environment and reduce building energy consumption, but its use is challenging in urban areas due to the heat island, reduced wind speeds, air pollution and noise (Ghiaus, Allard, Santamouris, Georgakis, & Nicol, 2006; Martins & Carrilho da Graça, 2017).

CONTACT P. F. Linden pfl4@cam.ac.uk

The objective of the Managing Air for Green Inner Cities (MAGIC) project is to break this vicious cycle by developing an advanced computational system that can be used to predict the airflow and air quality in a city in order to optimize the use of natural ventilation in buildings, thereby reducing energy demand and GHG emissions. An integrated management and decision-support system is being developed to achieve this, comprising:

- a fully resolved air-quality model that simulates the air flow and pollutant and temperature distributions in complex city geometries, fully coupled to observations, naturally ventilated buildings, and green and blue spaces;
- fast-running models that allow rapid calculations for real-time analysis and emergency response; and
- a cost–benefit model to assess the economic, social and environmental viability of planning options and decisions.

The key requirement is that output is of sufficient quality and resolution to support decisions that provide high-quality indoor environments using natural ventilation in place of air-conditioning, thus reducing energy demand and emissions from the built environment. Experiments and simulations of selected city stereotypes in different local climate zones (Stewart & Oke, 2012) are planned to support the first two points above, and here we describe the initial phase of that activity.

To examine the potential of natural ventilation under the challenges of both the urban heat island and air pollution, the MAGIC team conducted experiments and simulations for both the indoor and outdoor environments at a test site. The research team monitored air quality indoor and outdoors, used wind tunnel experiments and computational fluid dynamics (CFD) to simulate the outdoor environment, with internal modelling to treat the indoor environment and the indoor–outdoor exchange. Accompanying this, water flume experiments were used to develop ways of improving the indoor modelling. The authors are developing reduced-order modelling (ROM) to enable rapid simulations that can be used in place of the computationally expensive CFD model, but which retain much of the fidelity of the CFD model. Methods are also being developed to assimilate data into the models so they can interpolate sensor data and generate good initial and boundary conditions from which simulations can predict into the future. A further use of these methods is to optimize the placement and type of sensors in the local environment. A schematic of the links between these activities – the MAGIC circle – is shown in Figure 1.

The field study consisted of external and internal air quality measurements over a five-month period, the latter within a naturally ventilated office room in the Clarence Centre (51°29′54.38″N, 0°6′14.9″W) in the Borough of Southwark, London (Figure 2). The study area is categorized as a compact, mid-rise, urban local climate zone (Stewart & Oke, 2012), including a modest number of high-rise buildings and affected by air pollution from intensive traffic flow. A naturally ventilated room on the top floor of the three-storey test building was selected for the study (Figure 3(a)). It is connected to two adjacent naturally ventilated rooms (the four windows to the left in Figure 3(a)) and has simple window configurations with two windows facing a busy road (London Road), one window facing a traffic-free courtyard and a skylight in the ceiling. A number of natural ventilation

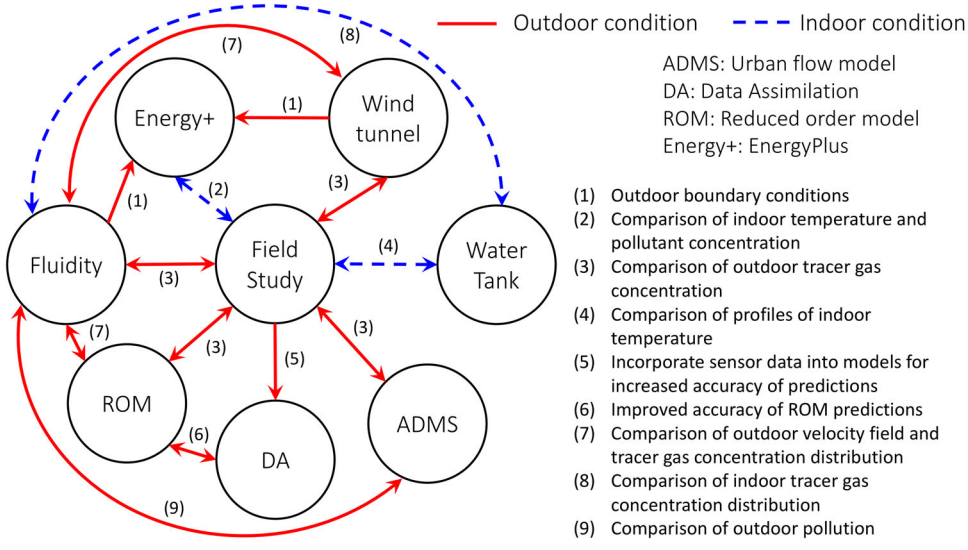

Figure 1. Schematic of the Managing Air for Green Inner Cities (MAGIC) Circle.

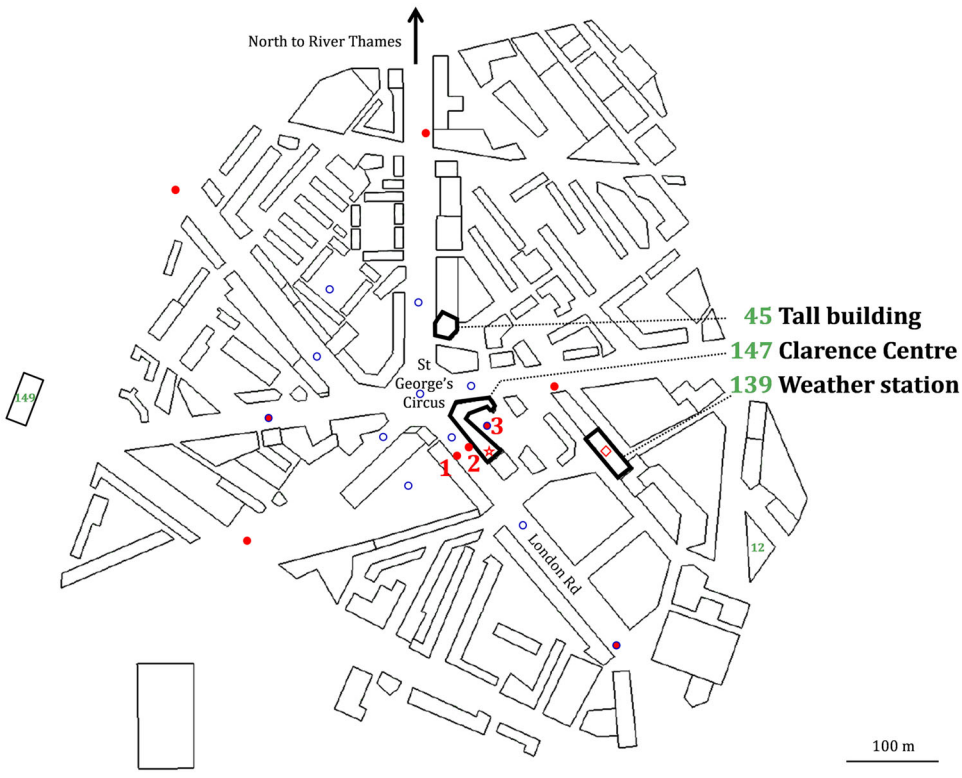

Figure 2. Outdoor sensor network and wind tunnel data points: filled red circle, MAGIC monitor; star, test room in Building 147 (outlined in bold); diamond, weather station (building outlined in bold); and open blue circle, measurement positions in wind tunnel and Fluidity.

types can therefore be investigated, including single-sided ventilation (SSV, openings on one facade), cross-ventilation (CV, openings on opposite facades) and stack ventilation (SV) due to buoyancy (Daish, da Graça G., Linden, & Banks, 2016; Linden, 1999; Mateus & Carrilho da Graça, 2015).

The paper is structured as follows. The next section describes the methods employed in the research. This is followed by a section presenting the main results, including a discussion of the influence of the outdoor urban environment on the natural ventilation potential and the impact of the urban configuration and buildings. The following section describes the ROM and data assimilation work, and includes studies under way to understand the level of detail that needs to be included in the modelling. Finally, conclusions and future work in the next phase of MAGIC are given.

Methods

Full-scale field experiment

To monitor the indoor and outdoor environment, the research team designed its own monitor units with six sensors, which enabled simultaneous measurements of carbon dioxide (CO_2), carbon monoxide (CO), nitrogen dioxide (NO_2), temperature, relative humidity (RH) and barometric pressure to be made. The CO and NO_2 sensors (Alphasense Ltd, UK) operate on an electrochemical principle. The CO_2 sensor (Senseair AB, Sweden) operates on a non-dispersion infrared method that determines CO_2 concentration based on light absorption (Mead et al., 2013). Each unit is powered by a rechargeable lithium battery with a low-power microcontroller and a power-saving routine to minimize power consumption. The sampling outputs were saved in a memory chip with a typical time interval of 30 s and downloaded through a USB interface. All units were calibrated before deployment by placing them side by side in ambient conditions monitored with reference instruments. Each unit is lightweight (less than 500 g), compact (circuit board dimensions of $10 \times 8.4 \times 2.8$ cm) and low cost (less than £1000), which allowed a denser sensor network than more expensive and bulkier units to be deployed (Figure 4).

Between August 2017 and January 2018, 18 monitors (nine indoors and nine outdoors) were deployed in and around the case study building. The outdoor network covered most major roads within a radius of 300 m of the test room, denoted by filled red circles in Figure 2. To characterize the outdoor environmental conditions on the two sides of the test room (*i.e.* London Road side and courtyard side) (Figure 3(a)), three monitors

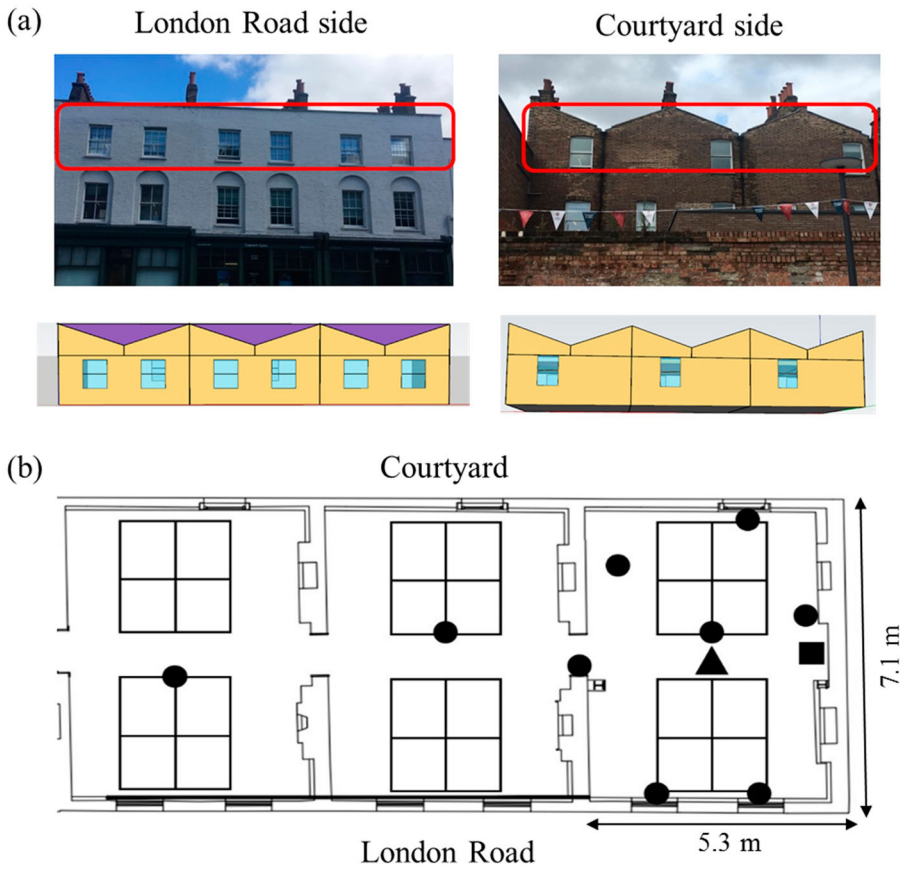

Figure 3. (a) The test room and its geometrical representation in EnergyPlus; and (b) locations of the indoor sensors.

were deployed close to the test room, with monitors 1 and 2 along polluted London Road and monitor 3 in the relatively clean courtyard. Another monitor was located approximately 650 m from the test room at the Elephant and Castle air quality monitoring station

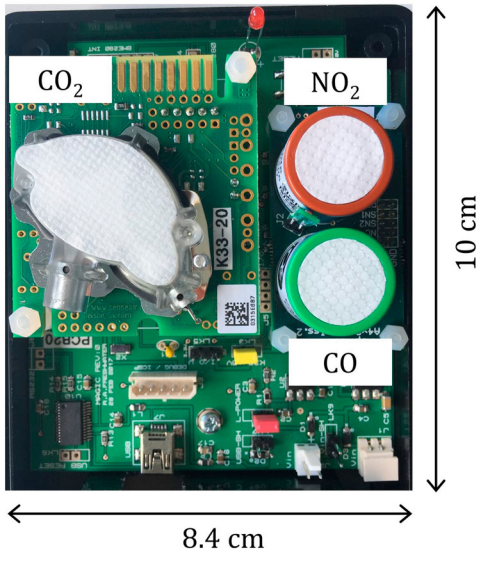

Figure 4. MAGIC monitor circuit board.

with a reference NO_2 instrument. In addition, a meteorological station with a weather station package (Met-Pak, Gill Instruments Ltd) and a solar pyranometer (SPN1, Delta-T Devices Ltd) was installed on the rooftop of the nearby eight-storey Building 139 (denoted by a red diamond in Figure 2) to record local wind speed, wind direction, temperature, RH and barometric pressure (all at 1 Hz), as well as total and diffuse solar radiation every 10 min.

Inside the case study building, the sensor network was deployed with seven monitors in the test room and two monitors in two adjacent rooms, connected to the test room via open doorways (Figure 3(b)). The monitors in the test room were arranged to capture spatial variations in locations of particular interest such as the windows/skylight and in the room centre/edge. A floor-to-ceiling vertical array of eight temperature sensors (PT100 Pico SE017) was also deployed in the test room to measure the vertical temperature stratification. The temperature sensors were calibrated by a co-location test before deployment with additional on-site calibration and data collection at 1 Hz by two PT-104 PicoLog data loggers connected to a laptop. Finally, a 180° fisheye camera was mounted on the

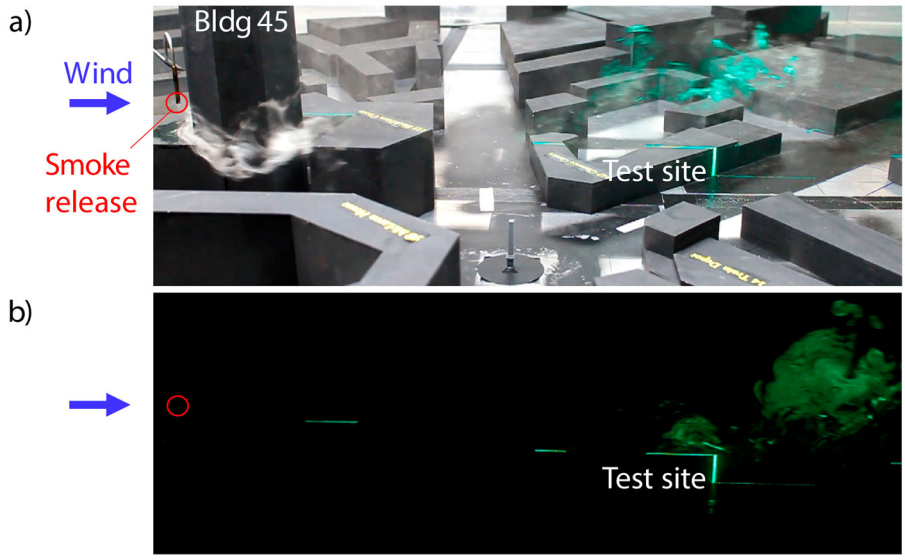

Figure 5. Wind tunnel visualization of smoke advected over the test site by the wind and illuminated by a green laser light-sheet.

ceiling to monitor the number of occupants and window opening sizes.

Wind tunnel experiments of the external flow

The flow and pollutant dispersion over the test site was simulated in the EnFlo Meteorological Wind Tunnel (working section of 20 m length and 3.5×1.5 m^2 cross-section), which can be used to simulate a range of atmospheric stability conditions. The neutrally stable boundary layer approach flow was developed with standard Irwin spires and staggered rows of distributed roughness elements along the initial 12 m fetch of the wind tunnel. The stream-wise mean wind velocity conformed to a standard profile shape for a turbulent boundary layer over suburban terrain (power-law exponent of 0.19 ± 0.01). The free-stream mean velocity was maintained steady, within $\pm 0.5\%$ of the set-point. The 1:200 scale model of the urban site included buildings within approximately 300 m of the test building with prominent peripheral high-rises within 500 m added for westerly (W; Building 149) and south-easterly (SE; Building 12) winds (Figure 2). The geometry was extracted from a digital map and database (MasterMap; Ordnance Survey, 2016). Buildings were simplified to 149 cuboids by extruding their general footprints to the most reliable measured height (ground to base of roof; Ordnance Survey, 2014). The first set of experiments used flat-roof buildings; later work examined the importance of roof shape and the impact of individual high-rise buildings. The approaching wind direction was controlled over the full compass range, within $\pm 0.25°$, by automated turntable positioning of the model using an overhead camera and image correlation.

Smoke flow visualization (Figure 5) provided an overview of flow conditions and highlighted specific features, such as the wake of the tall Building 45. A two-component laser Doppler anemometer (2D-LDA; Carpentieri, Hayden, & Robins, 2012; Durst, Melling, & Whitelaw, 1976) provided quantitative measurements of mean and fluctuating air velocity with a typical sampling rate of 50 Hz. The instrument was used in two alignments in order to obtain three flow components. Dispersion studies used a passive hydrocarbon tracer, the concentration of which was measured with a fast-flame ionization detector (FFID) with a frequency response near 200 Hz (Carpentieri et al., 2012; Fackrell & Robins, 1982). Turbulent mass fluxes were determined by simultaneous LDA and FFID measurements. The external surface pressure distribution on the model Clarence Centre (Building 147) was measured by 88 pressure taps on the roadside, courtyard side and roof of the test site model. Each tap was connected to a pressure transducer by 400 mm of 1 mm internal diameter plastic tubing. Pressures were measured with transducers (RSCDRRM2.5MDSE3, Honeywell International) at 200 Hz, this being about twice the frequency response of the transducer. No interference from Helmholtz resonance in the tubing system was observed.

CFD simulation

CFD simulations were carried out for the study area using Fluidity, an open-source, finite-element, fluid dynamics model (see http://fluidityproject.github.io/). A large eddy simulation (LES) approach was used to represent turbulence. The LES equations describing the turbulent flows were based on the filtered incompressible Navier–Stokes (NS) equations (momentum equations and

continuity of mass). In addition, a sub-grid-scale model based on the anisotropic eddy viscosity was used to close the equations. The dispersion of pollutant is described by the classic advection–diffusion equation with the pollutant concentration treated as a passive scalar. A source term was added to the advection–diffusion equation to mimic a constant release of pollutant. All the equations were solved using second-order schemes in time and space. The NS equations were discretized using a continuous Galerkin discretization, while the advection diffusion was discretized using a coupled finite-element/control-volume method. The time step was adaptive based on the courant (CFL) number defined by the user, and the Crank–Nicholson scheme was used for the time discretization. For details of the equations and their implementation, see Ford et al. (2004) and Aristodemou, Bentham, Pain, and Robins (2009).

The mesh was unstructured (Figure 6), anisotropic and adaptive, which can be refined automatically in regions of interest during a simulation (Pain, Umpleby, De Oliveira, & Goddard, 2001). The mesh was constrained by three parameters given by the user: the maximum number of nodes, and the minimum and maximum edge length of elements. The mesh adaptivity can be field specific, so that the mesh refines based on different computed fields. In the simulations presented in this paper, field-specific adaptivity options were assigned to the tracer field and the velocity field.

The outlet boundary condition was defined by a zero-pressure (no-stress) condition; perfect slip boundary conditions were applied at the top and on the sides of the domain and no-slip boundary conditions were applied on the bottom surface of the domain and all building facades. The properties of the fully developed boundary layer measured in the wind tunnel, *i.e.* the mean velocity profile, the Reynolds stresses profiles and the turbulence length-scale profiles, were used to set up the turbulent inlet boundary conditions using the synthetic eddy method (Pavlidis, Gorman, Gomes, Pain, & ApSimon, 2010). The numerical results were compared with the wind tunnel data to validate the simulations.

Modelling of internal conditions

The US Department of Energy building simulation tool EnergyPlus (see https://energyplus.net) was used to quantify the effect of outdoor urban environmental conditions on internal conditions under natural ventilation. The model integrates building data (construction, materials and internal usage) and outdoor meteorological data (wind speed, wind direction, solar radiation, air temperature and air humidity) to simulate the indoor environment by considering indoor–outdoor exchanges of heat and pollution. The geometrical representation of the test room is shown in Figure 3(a); the methodology of EnergyPlus modelling is illustrated by Figure 7. External wind pressures coefficients on the test building facades were derived from both wind tunnel experiments and Fluidity simulations, both of which included the effects of surrounding building clusters. These wind-pressure coefficients determine the exchange through each window for a given wind speed (Daish et al., 2016). The results showed that the test site was significantly sheltered by its urban surroundings and that for many situations inflow was in the expected 'lee' of the test building rather than the side that was naively considered to be the windward based on the prevailing wind direction.

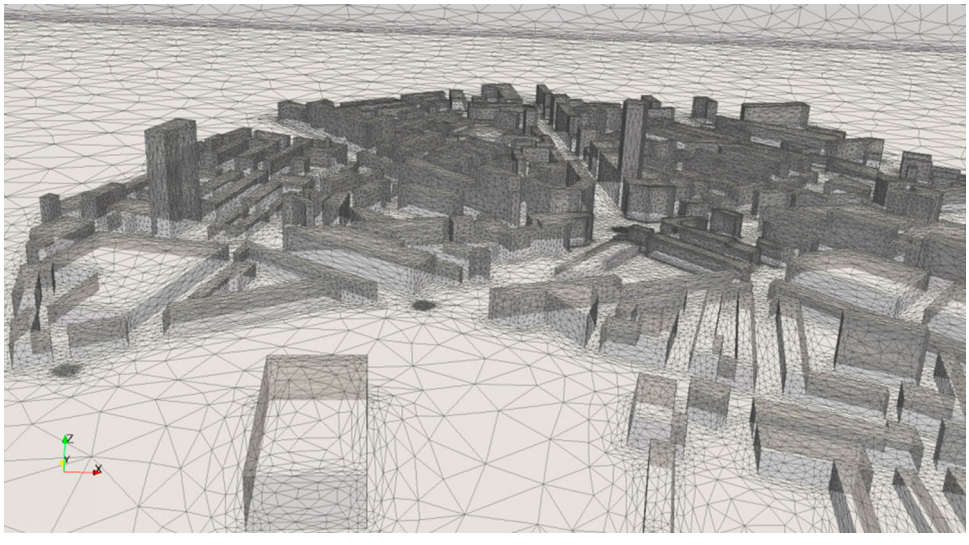

Figure 6. Initial unstructured mesh of the three-dimensional geometry of the test area.

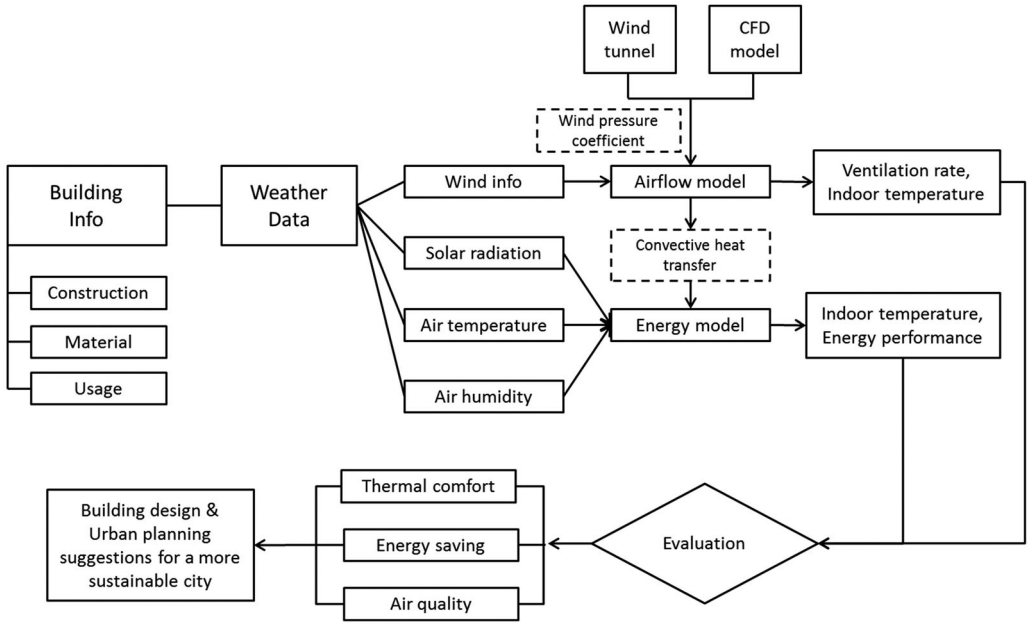

Figure 7. Schematic of the EnergyPlus model methodology.

Results and discussions

Evaluation of the EnergyPlus model

One week (25 September–1 October 2017) when the full set of indoor and outdoor observations was available was chosen to evaluate the EnergyPlus model. The data included air temperature and RH (Figure 8(a)), CO_2 and CO (Figure 8(b)), wind and solar radiation (Figure 8(c)), and the number of occupants and window-opening position (Figure 8(d)). Indoor temperatures (with a diurnal variation of 4.9°C) were usually higher than outdoor temperatures (with a larger diurnal variation of 11.9°C), possibly due to the thermal mass and air tightness of the building envelope. The variation of indoor CO_2 was found to be closely related to occupancy levels due to exhaled human breath, while the variations of outdoor CO_2 and CO were influenced by outdoor traffic with two concentration peaks coinciding with morning and afternoon rush hours.

The simulated and measured indoor averaged temperatures agreed well with the same trend and root mean square error (RMSE) of 1°C (Figure 8(a)). A possible cause of this RMSE might be the use in EnergyPlus of a single temperature that ignores spatial variations within the space, such as the vertical temperature stratification. Figure 9 shows an example of the diurnal development of the temperature stratification on 25 September 2017. Temperature stratification started to form at 09:00 hours when occupants first entered the test room with the air near the ceiling approximately 1°C warmer than near the floor. The room temperature increased until the window was opened at 15:00 hours, providing SSV and producing a reduction in room temperature and enhanced stratification. After the window was closed, the room began to warm again with increasing stratification until the occupants left at the end of the day, after which it cooled and gradually reached a well-mixed state at night. To characterize the indoor temperature stratification and spatial concentration variations, water flume experiments and indoor Fluidity simulations (described below) were conducted to assess the limitations of EnergyPlus.

Evaluation of Fluidity modelling

To examine the capability of Fluidity modelling and promote the understanding of wind and dispersion conditions at the site, we selected two areas around the test building (*i.e.* Building 147 in Figure 2): the central roundabout (the centre of the study domain; Figure 10(a)) close to the test building and a street canyon adjacent to the test building (*i.e.* on the London Road side; Figure 10(b)). The wind tunnel experiments revealed the flow to be complex, with recirculation and separation in street canyons, and deep and persistent wakes from the taller buildings. These regions of turbulent flow tested the modelling capability of Fluidity. We compared velocity profiles at these two locations from both the wind tunnel experiments and Fluidity simulations for a wind blowing from the north-west (NW). Wind velocity and height above the ground were normalized by the velocity at the top of the approaching boundary layer U_{ref} and the boundary layer depth δ respectively. The wind tunnel profiles were

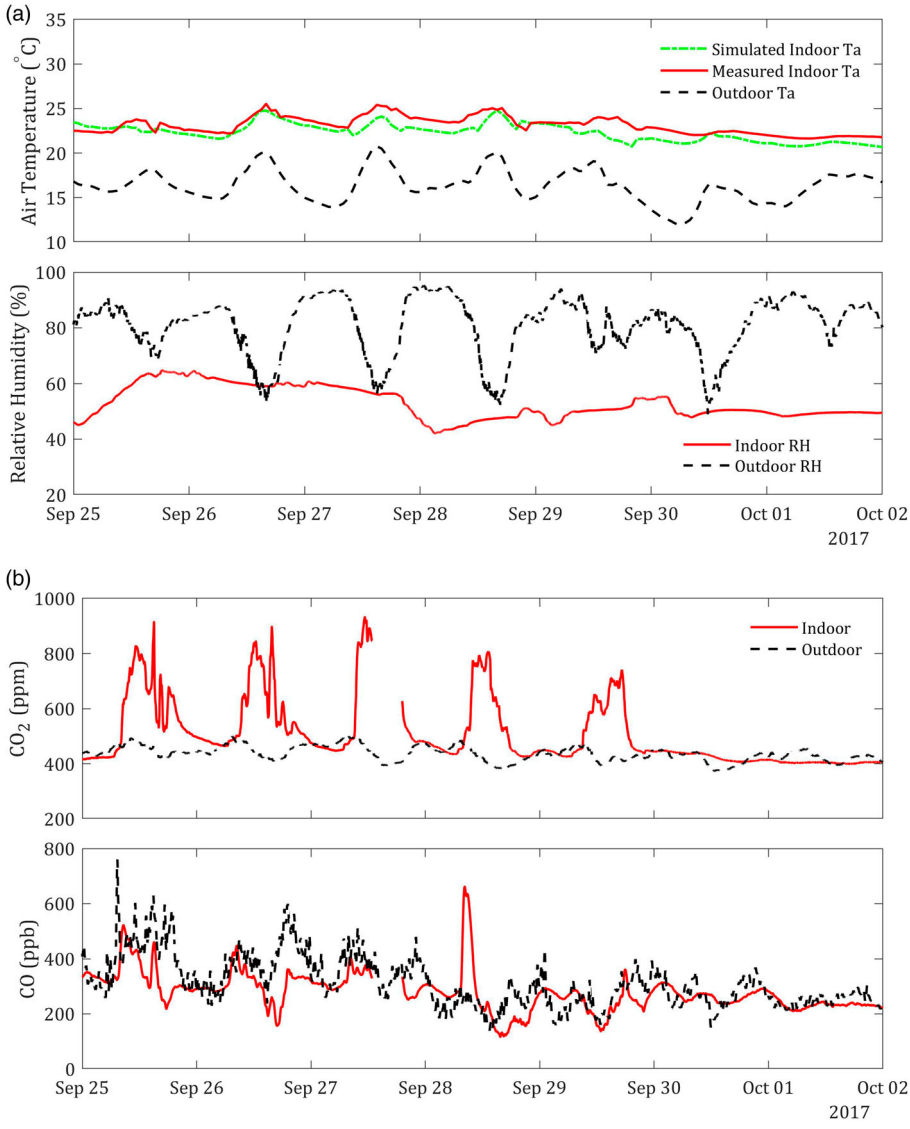

Figure 8. (a) Temperature and relative humidity measurements from 25 September to 1 October 2017; (b) CO_2 and CO measurements from 25 September to 1 October 2017; and (c) wind speed and direction, direct and diffuse radiation from 25 September to 1 October 2017.

reproduced by the Fluidity simulation reasonably well at the roundabout (Figure 10(a)). However, some discrepancies appeared between the roundabout and the street canyon of London Road (Figure 10(b)). Here, Fluidity underpredicted the stream-wise component, U_{mean}/U_{ref}, for $z/\delta < 0.15$, though this discrepancy diminished further along the street canyon (Figure 11). These discrepancies probably imply a lack of local model resolution and the results are expected to improve by refining the simulation resolution.

All the vertical profiles shown in Figures 10 and 11 show a canopy layer that is approximately 0.2–0.3δ in depth, and characterized by lower wind speeds than expected at the same height in the undisturbed approach flow. The depth of the canopy layer is between 40 and 60 m at full scale, chiefly influenced by the tallest upwind buildings; specific effects seen in the wakes of high-rise buildings are discussed below in the subsection entitled 'Impact of tall buildings'. The measured and simulated profiles converge in the upper part of the boundary layer, above about 0.5δ, tending towards the upstream flow conditions. Generally, although mean wind speeds at street level are low, the turbulence levels, when expressed in terms of local wind speeds, are generally larger in the canopy layer than in the upstream flow at the same height.

Impact of urban form

Wind tunnel dispersion experiments, using passive tracer gas released from a ground-level source at the central roundabout, were carried out to characterize on-site dispersion behaviour, and to provide additional data sets for use in evaluating Fluidity. A further objective was to

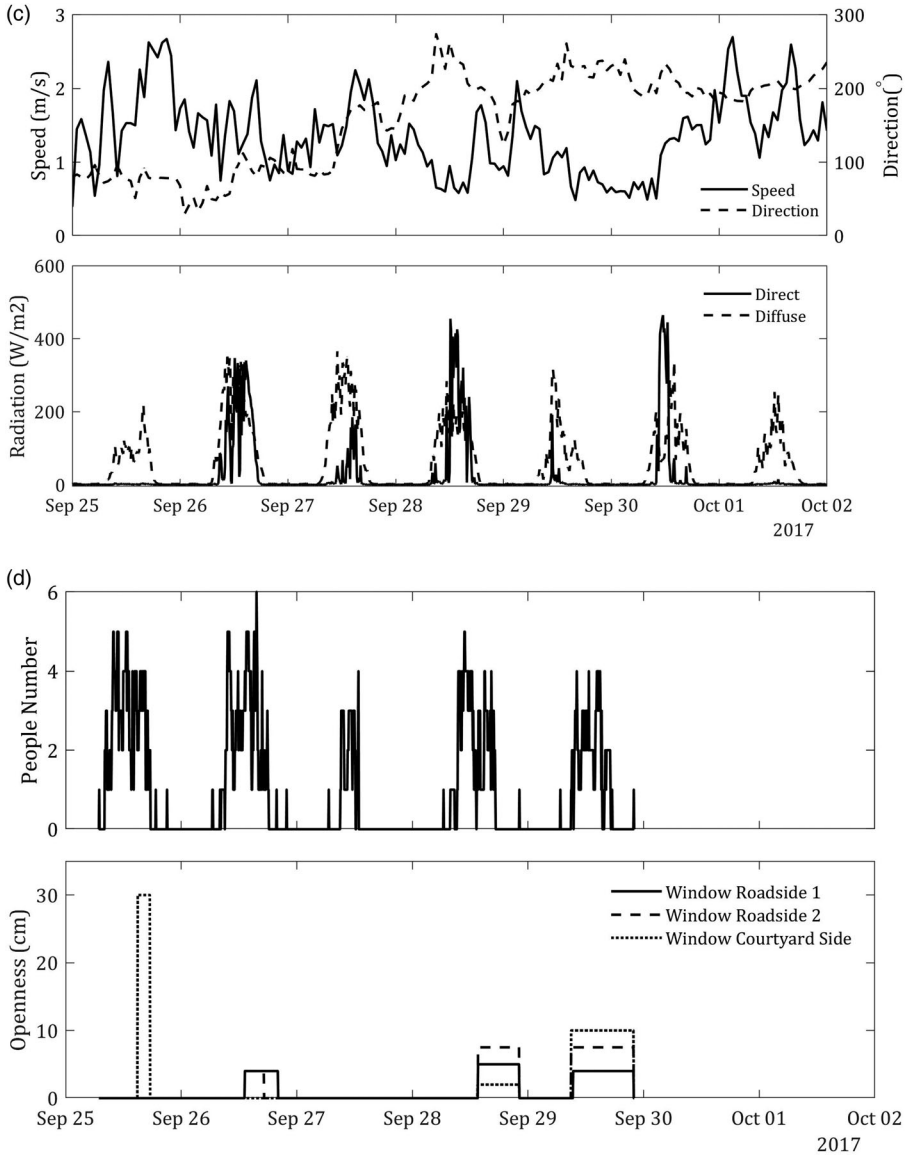

Figure 8. *Continued.*

compare behaviour with that previously observed in London at the Dispersion of Air Pollution and its Penetration into the Local Environment (DAPPLE) site in Marylebone Road (Arnold et al., 2004; Wood et al., 2009). The two sites have very different characteristics: the street pattern at the DAPPLE site is grid-like and the range of building heights is modest, whereas the MAGIC site has a predominantly radial street arrangement and a greater range of building heights. Dispersion behaviour will, of course, reflect these differences but, nevertheless, the decay of maximum mean concentration with radial distance from the source was very similar in the two cases, following an inverse-square form. This is a useful conclusion, showing the robustness of the empirical correlation developed during the DAPPLE experiments.

Dispersion behaviour in the prevailing wind directions (W and WSW) was simulated with Fluidity to illustrate dispersion conditions in the environment surrounding the test building (Building 147). In the examples shown, pollutant was released from point sources alongside the test building: one in the street canyon (London Road, L) and one in the courtyard (C). Example instantaneous tracer iso-surfaces and vertical profiles of non-dimensional mean pollutant concentration are shown in Figures 12 and 13(a, b). Concentrations are normalised using:

$$C^* = CU_{\mathrm{ref}}H^2/Q,$$

where C^* is the normalised concentration (dimensionless), C is the concentration (mg/m^3); U_{ref} is the reference wind velocity (m/s); H is the average building height (m); and Q is the pollutant emission rate (mg/s). A strong sensitivity to wind direction and source

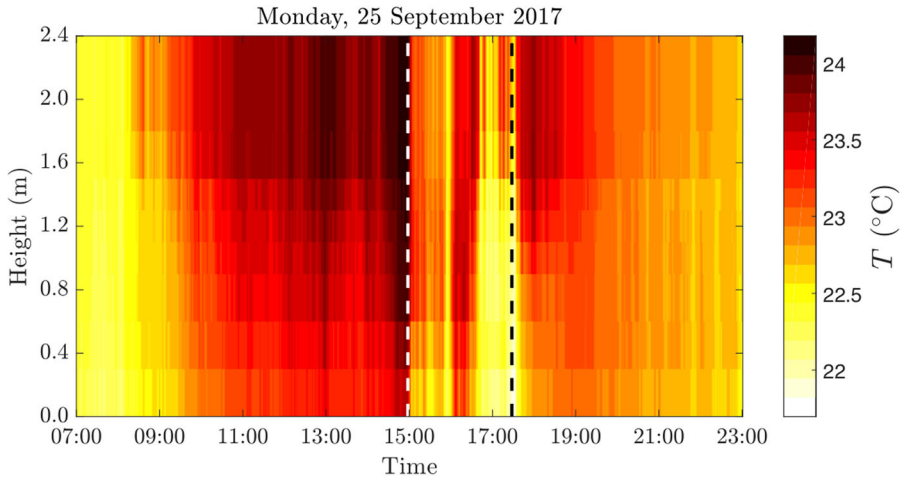

Figure 9. Measurements from the temperature array: stratification formed at 09:00, filling the room by 11:00; and the temperature falling when the window on the courtyard side was open between 15:00 and 17:30 hours (dashed lines).

location is clear. Features of note include dispersion along London Road (source L, W wind), dispersion into the courtyard (sources L and C, W wind), dispersion away from the courtyard (source C, WSW wind), as well as the differences in extent and depth between the W and WSW wind cases. The flow over and in the wake of Building 147 dominates dispersion in the near-field, as is clear from Figure 13(a, b). Overall, cross-wind dispersion in the street network driven by the urban geometry can be substantial, and can take plume material far from the nominal plume centreline based on the mean wind direction above roof level. This, too, was a feature of dispersion at the DAPPLE sites, where plumes from road-level sources often spread across a 90° sector.

Impact of tall buildings

Heist et al. (2009), Brixey et al. (2009) and Aristodemou et al. (2018) illustrate some of the important effects of a single large building on the urban flow field. Broadly speaking, down-flow on the front face of the building leads to outward flow in the streets upwind and often an intensification of the vortex in the street canyon immediately upwind, whereas up-flow on the back face leads to inward flows in the streets downwind. A wake region of reduced wind speed and enhanced turbulence levels persists over several building diameters downwind.

To illustrate the impact of tall buildings at the MAGIC site, a prominent building (Building 45; Figure 2) was selected as an example. The effect of the building wake is clearly observed experimentally and well predicted numerically. In the wind tunnel experiment, lateral profiles of velocity downwind revealed an extended wake region of mean velocity deficit and increased turbulence intensity. Comparison of the wind tunnel experiment and the Fluidity simulation of the lateral profiles of the normalized mean velocity components at half-building height in the wake of Building 45 are shown in Figure 14. Two main zones can be identified: a deficit region downstream of the building and two disturbed regions to the sides. The behaviour of the three components suggests vertical recirculation at this height.

The wake behind an isolated tall building was clearly detectable at a downwind fetch of four building heights, that is, approximately 400–500 m for the buildings affecting the MAGIC site. The wake is characterized by a velocity deficit and enhanced turbulence. As can be seen in Figure 14, wakes become quite wide downwind and continue to spread as they decay. It is therefore likely that wakes from just a few tall, upwind buildings may combine to create an extensive region of velocity deficit, so that not only will the flow over the downstream region be reduced but also it will be far from being a classical boundary layer, making its specification in standard operational dispersion models particularly difficult.

Some outstanding modelling issues

The question of what level of detail to include when modelling flow and dispersion in an urban area is unanswered. It is, of course, quite clear that dispersion at the microscale is dependent on features such as building and street geometry, but details of roof geometry are often ignored with buildings modelled with flat roofs, as is the case in the basic model of the test site. Further, traffic induced flow and turbulence may be important, particularly in low wind speed conditions (*e.g.* Badas, Ferrari, Garau, & Querzoli, 2017; Brown, Lawson, DeCroix, & Lee, 2000; Yassin, 2011).

The effect of roof geometry on flow and dispersion over the MAGIC site is being investigated as part of

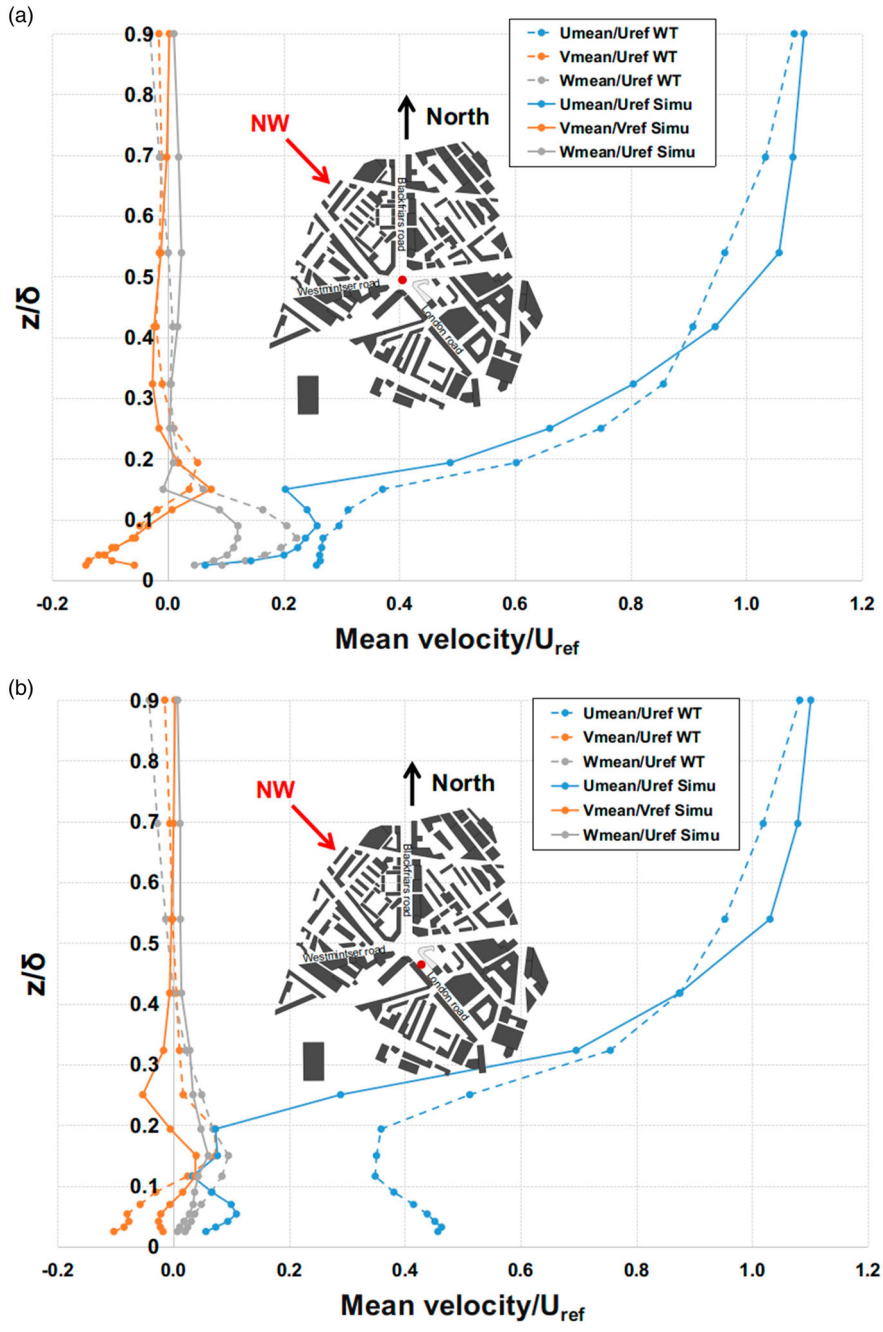

Figure 10. (a) Comparison of normalized mean velocities from the wind tunnel (dashed lines) and Fluidity (solid lines) for vertical profiles in the centre of the domain; and (b) comparison of normalized mean velocities from the wind tunnel (dashed lines) and Fluidity (solid lines) for vertical profiles in London Road.

the wind tunnel work. Here, though, the focus is on results from Fluidity simulations for the simple case of turbulent flow over two parallel canyons. As in the main body of Fluidity work, the Synthetic Eddy Method (Pavlidis et al., 2010) was used to develop turbulent inlet boundary conditions that matched the fully developed boundary layer flow in the wind tunnel. A $3.5 \times 4 \times 2$ m^3 domain representative of a wind tunnel was used and simulations run with street canyons aligned at 90 and 100° to the wind direction (*i.e.* normal and slightly off-normal to the mean flow). The geometry of the first building was fixed as a flat roof in all simulations and building height-to-canyon width ratio was $H/W = 1$. The geometries of the second and third building were varied in order to investigate the effect on the flow within the second canyon. Three geometries were used: (a) a pitched roof, $H/W = 1.5$, (b) a flat roof, $H/W = 1$ and (c) a flat roof, $H/W = 1.5$ (Figure 15).

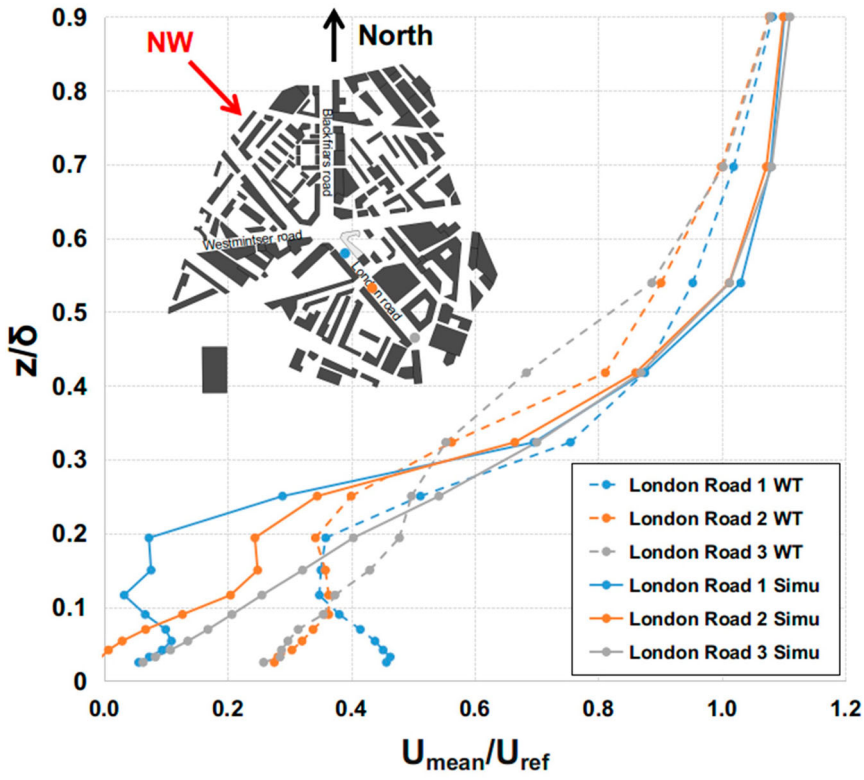

Figure 11. Comparison of the normalized mean stream-wise velocities from the wind tunnel and Fluidity for three vertical profiles located along London Road. Solid lines: Fluidity results; and dashed lines, wind tunnel data.

A passive tracer was released near ground level at the centre of the second canyon. Figure 16 shows the time-averaged normalized tracer concentration when a quasi-steady state had been reached. It can be seen that in cases (a) and (b), the orientation of the street canyon has little effect on tracer dispersion. However, in (c), tracer is dispersed much further along the canyon. In (a) and (b) tracer is more readily mixed into the flow

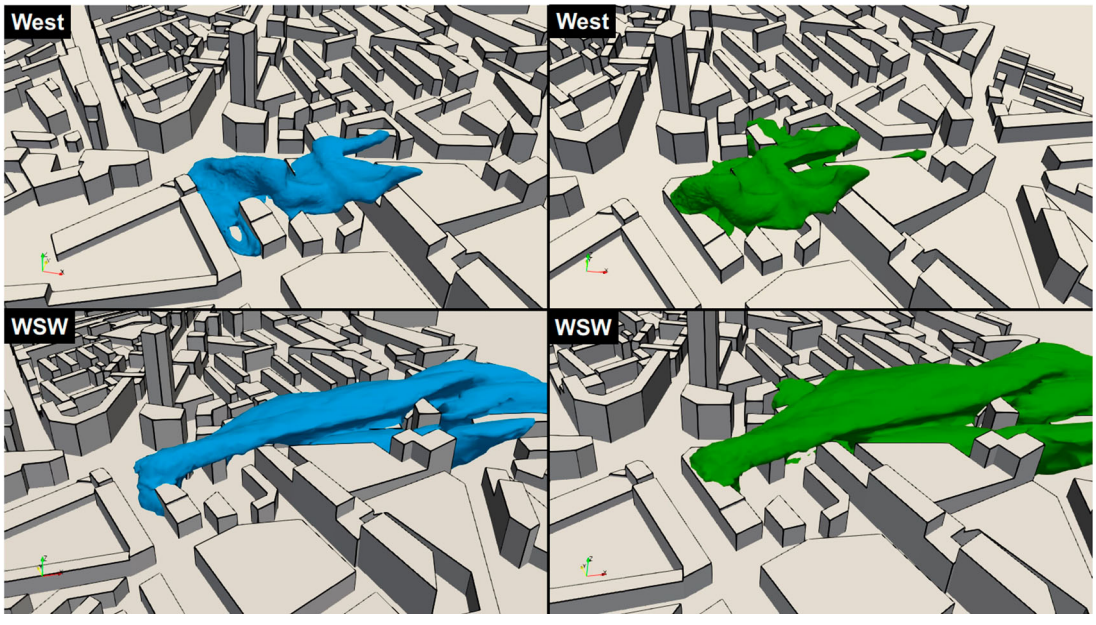

Figure 12. Snapshots of the dispersion of two passive tracers for wind from the west and west-south-west (WSW). Blue and green iso-surfaces correspond to sources located on London Road or courtyard sides, respectively. Iso-surfaces correspond to a normalised pollutant concentration (C^*) of 0.1.

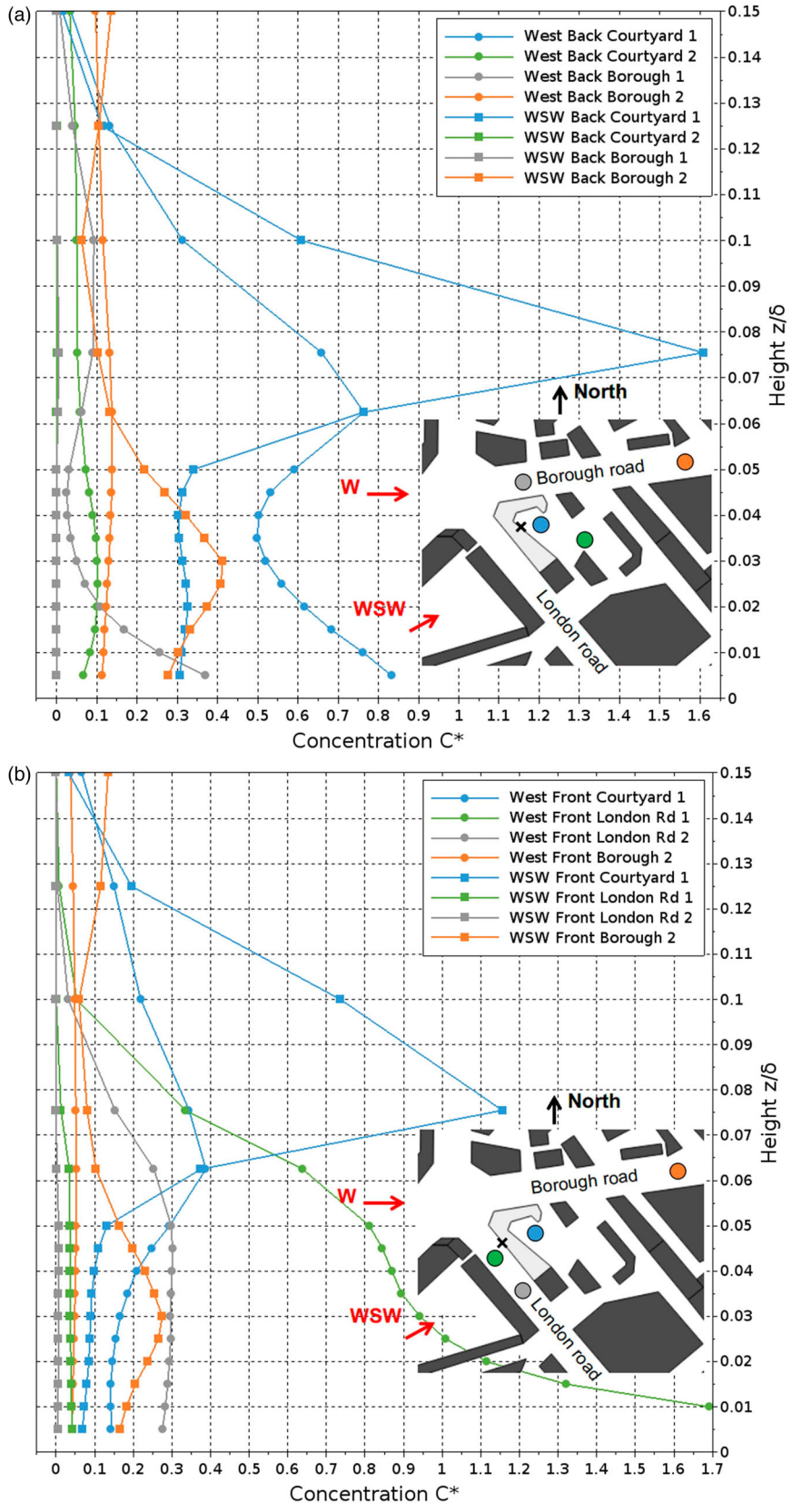

Figure 13. (a) Vertical profiles of dimensionless mean concentration for sources at the courtyard side. Black crosses denote source locations.

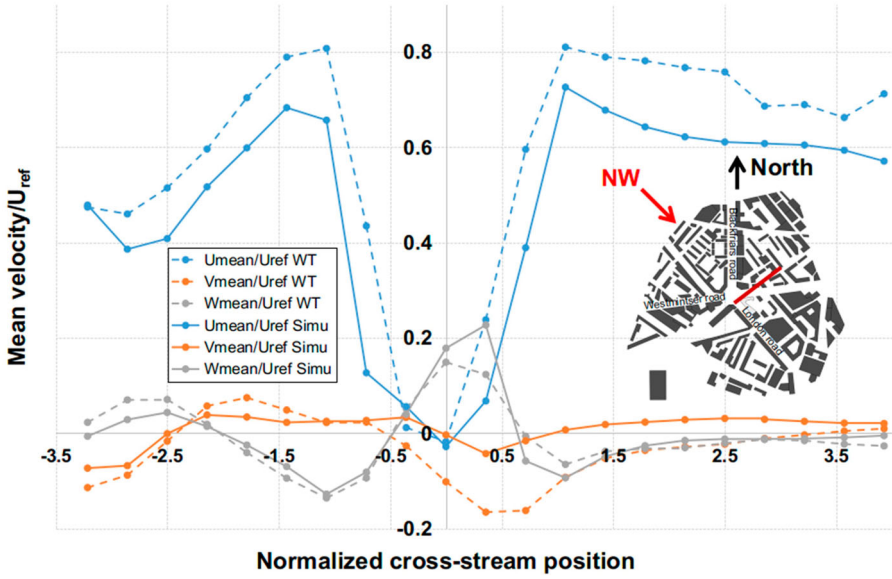

Figure 14. Comparison of the normalized mean velocities along a horizontal profile at half building height in the wake of the tall Building 45. The profile is from south-west to north-east. Distances are normalized by the width of the building.

above the rooftop, limiting along-canyon dispersion. Upwind dispersion of the tracer into the adjacent canyon is seen in (b). There were significant differences between the pitched and flat roof cases for both orientations.

During DAPPLE, experiments in the region around Marylebone Road (Arnold et al., 2004; Wood et al., 2009), concentrations of a released tracer were observed at locations well upwind of its source, the likely dispersion process being transport of the tracer by traffic-induced flow. Vehicle motion and emissions can be simulated by the traffic model in Fluidity (Garcia et al., 2011). Vehicles are modelled as a highly viscous slug (effectively a solid) and Fluidity adapts the mesh to capture the interface between moving vehicles and the air. As the vehicle velocities are predefined, the NS equations are solved only for air, with additional momentum source and absorption terms for the force applied by a vehicle on the surrounding air. A traffic simulation was run using Fluidity to demonstrate the effect on dispersion, in which a bus travelled upwind along a street canyon at 10 ms^{-1} (Figure 17). The wind speed was constant at 3 ms^{-1}. Tracer released at the centre of the canyon formed a cloud through which the bus passed. Figure 17 shows a tracer iso-surface, corresponding to a normalized concentration of 0.1, 10 s after the bus passed through the cloud, clearly demonstrating pronounced upwind transport.

Modelling enhancements

Reduced-order CFD simulation

Resolving much of the detailed air flows and associated transport of pollution within cities is extremely

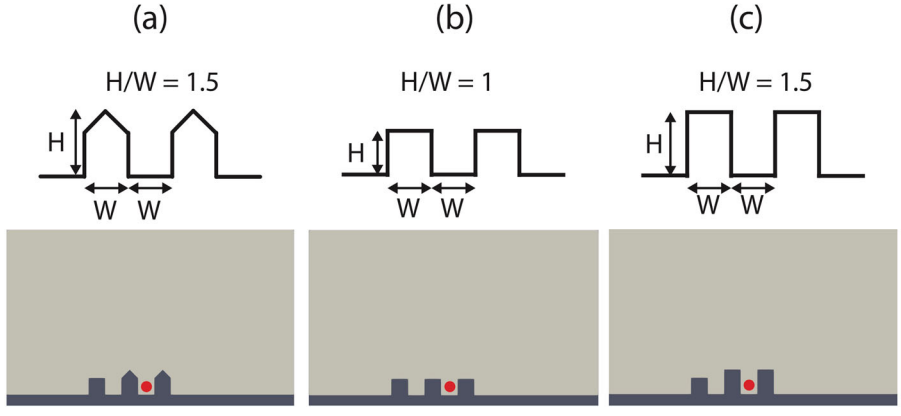

Figure 15. Street canyon geometries: (a) pitched roof; (b) flat roof set at the base height of the pitched roof; and (c) flat roof set at the ridge height of the pitched roof. The location of the tracer source is shown in red.

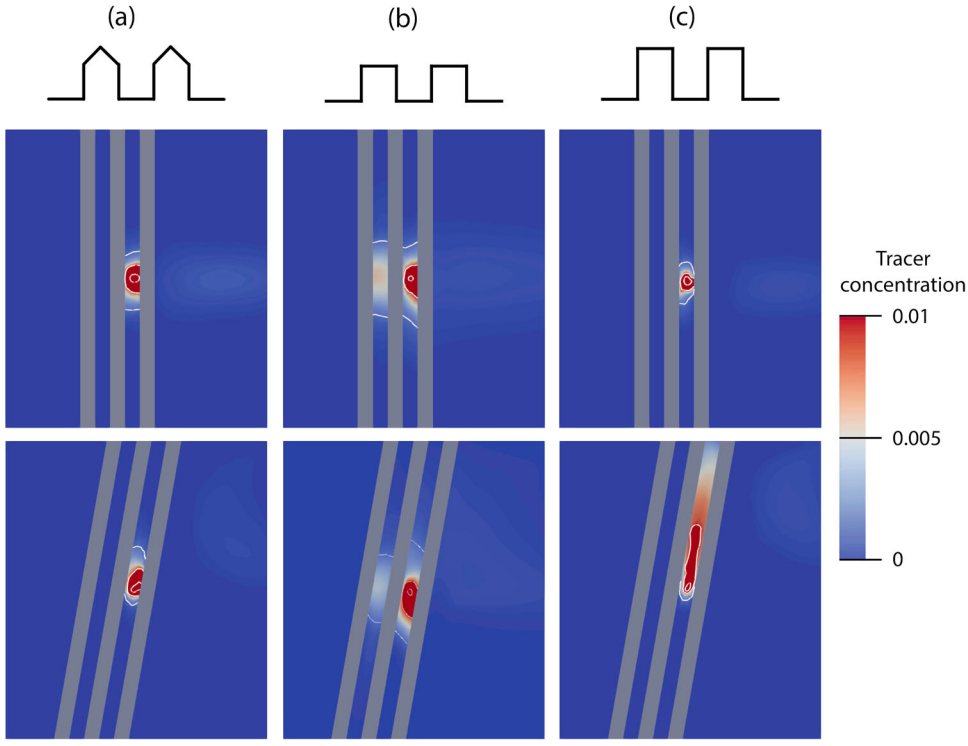

Figure 16. Time-averaged, normalised concentration (C^*) of tracer released at the centre of the second street. Cross-sections are taken at the height of the tracer source H/4.

computationally intensive. It is currently impossible to model the system sufficiently quickly to be able to predict behaviour in real time or assess risks adequately. An aim of this study is to demonstrate a key step towards the use of a ROM for operational purposes, with the tantalizing possibility of it being used in place of a Gaussian plume or related models for practical applications. This could provide greatly improved model fidelity and confidence for air flow and pollution modelling in urban environments.

There are three aspects to producing an operational model: (1) an ability to predict the full-model results using a non-intrusive reduced order model (NIROM); (2) an ability to have a model with similar dynamics that can be run as long as one likes and has similar dynamics to the full model and which can predict from different initial conditions; and (3) a model that is parameterized and takes varying forcing from boundary conditions, physics such as temperature variation *etc.* The NIROM is based on deep-learning methods and proper orthogonal decomposition (POD). The key idea is that deep learning is used to construct a set of hypersurfaces, representing the reduced system (including linear and non-linear processes). The novelty of the method rests in how the ROM is generated, *i.e.* how the hypersurfaces are calculated using a long short-term memory network (LSTM) (Wang et al., 2018). Previous research (Xiao et al., 2014; Xiao, Fang, Pain, & Navon, 2017) has shown that the predictive accuracy of a ROM is maintained while central processing unit (CPU) costs are reduced by several orders of magnitude. Figure 18 shows the flow around the test site using the full Fluidity simulation (left) and ROM (right). The ROM was constructed from the first 27.5 min of the Fluidity simulation. It used 48 POD basis functions and ran in 31 s on a laptop (excluding time spent on input and output), compared with the 215 h that the Fluidity simulation took to run on 10 cores. Figure 18 shows the ROM is in excellent agreement with the full simulation. Future work will focus on developing a domain decomposition ROM which will form the basis functions within subdomains, thereby identifying the POD functions more efficiently. This method will also allow a ROM to be generated region by region without solving the full model across the whole domain.

Data assimilation

Pollutant concentrations and wind conditions monitored in urban areas are used to characterize environmental conditions and to examine dispersion model performance. Direct interaction between observations and predictions, aimed at improving the latter, is an emerging and potentially very powerful use of these data. The formal process is termed 'data assimilation'.

A data-assimilation technique, illustrated schematically in Figure 19, is being integrated with the Fluidity

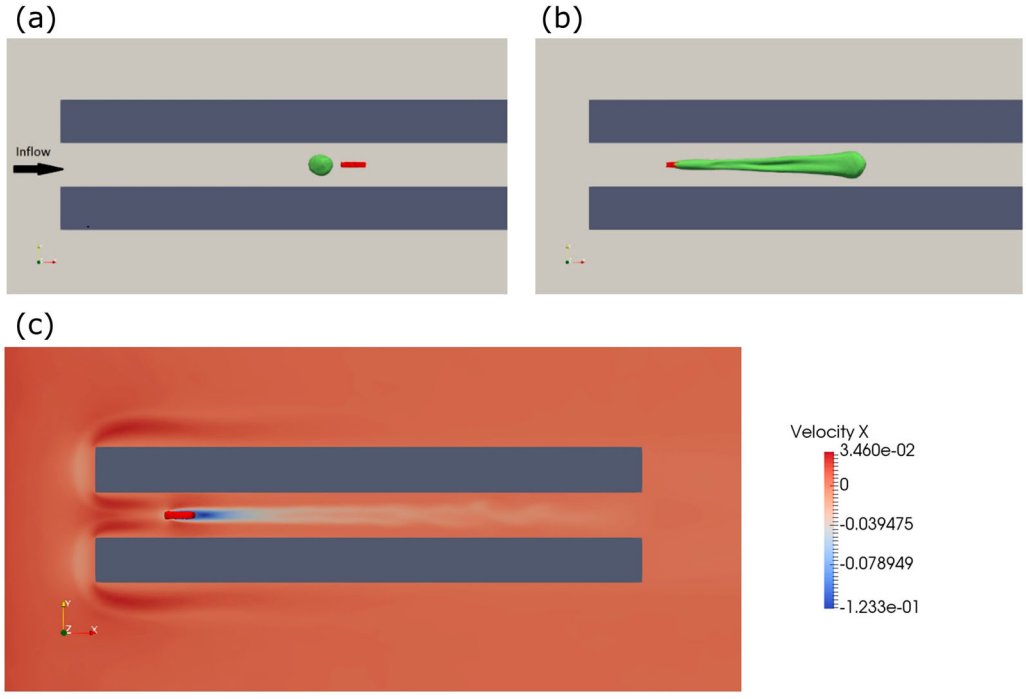

Figure 17. Simulation of a bus travelling upwind within a street canyon. In (a) the bus is about to reach a cloud (green) of passive tracer released at ground level in the canyon centre. In (b) the bus has travelled approximately 70 m further, carrying tracer with it. (c) Velocity field at half height of the bus; upwind velocities in the wake are clear.

model (in the full or ROM form). This is an uncertainty quantification technique used to incorporate observed data into a predictive model in order to improve numerical forecasts (Kalnay, 2003). The approach implemented is variational data assimilation (Andersson et al., 1998; Baker, Huang, Guo, Bourgeois, & Xiao, 2004), first developed for weather forecasting and based on the minimization of a cost function that estimates the discrepancy between numerical results and observations, assuming that both forecasts and observations contain errors that can be adequately described by error covariance matrices (Kalnay, 2003). The greatest challenge in developing the framework of data assimilation is the ill-conditioned nature of the background covariance matrix. To reduce noise in the prediction generated by data assimilation, the

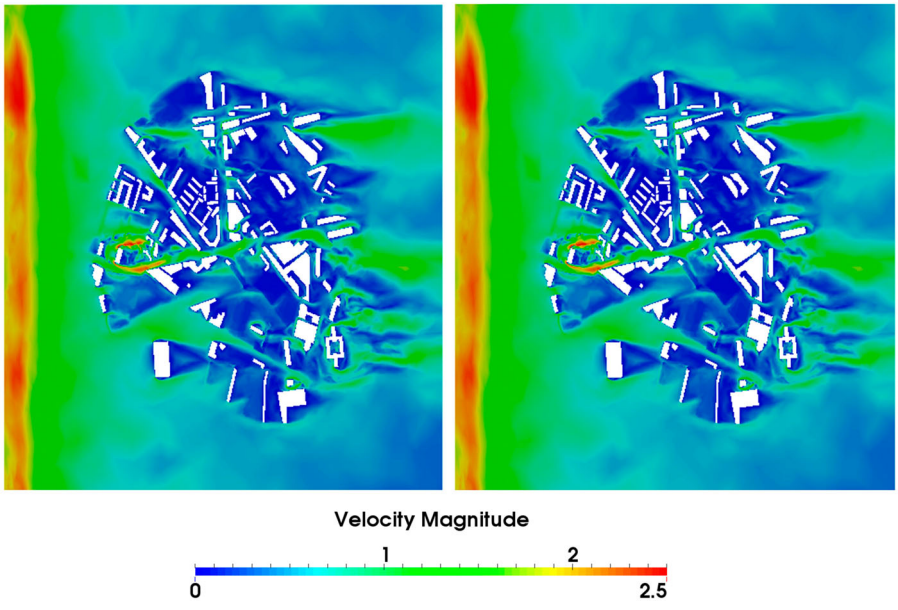

Figure 18. Comparison between full Fluidity simulation of the test site and reduced order model (ROM) at one instant: (left) full simulation; and (right) ROM. Colour indicates velocity magnitude (m s^{-1}). Flow is from left to right.

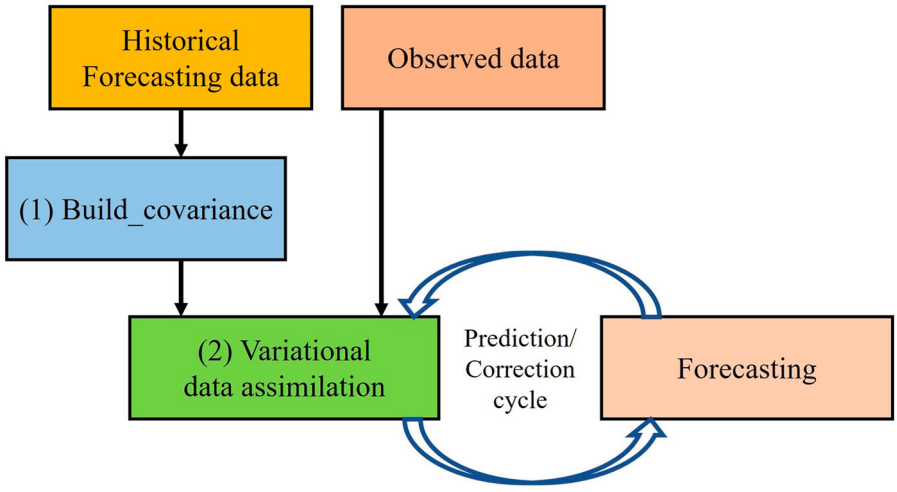

Figure 19. Schematic of the data assimilation framework in MAGIC.

empirical orthogonal functions (EOF) method (Lorenz, 1956) is used. EOFs strongly reduce the dimension of the problem, alleviating computational cost, but a consequence is that important information can be missed (Cacuci, Navon, & Ionescu-Bujor, 2013). The present paper has shown, using pressure and velocity fields from Fluidity simulations, that by selecting the mean of the maximum and minimum singular values of the background error covariance matrix as the regularization parameter, the computational cost can be minimized without significant loss in solution accuracy.

Water flume experiment (laboratory-scale indoor experiment)

Water flume experiments with a simplified, scaled geometry will be used to help build simple theoretical models of ventilation processes. Using water provides compelling flow visualization of the indoor–outdoor exchange that is not available by other methods (Linden, 1999), and allows appropriate modelling of buoyancy forcing but with Reynolds numbers necessarily smaller than at full scale. Fluidity simulations were performed to identify whether the reduction in Reynolds number had any serious impact on flow conditions. Full-scale simulations represented a cross-ventilated room (5.4 m wide, 7.4 m long, 2.7 m high) in a large domain (21.6 × 35 × 5.4 m^3), with air as the working fluid and an inlet velocity of 1 m s^{-1}. Computational simulations at the 1:10 laboratory-scale used water as the working fluid and an inlet velocity of 2 cm s^{-1}; the Reynolds number was approximately 50 times smaller than in the air simulation.

In these simulations, the indoor and outdoor temperatures were equal. The room was initially filled with a passive tracer that was then flushed out by CV. The simulations used an adaptive mesh, with a 5 cm minimum edge length (5 mm in the water simulation), chosen such that the evolution of the mean pollutant concentration in the room converged. An appropriate dimensionless time is $\tau = tU/L$, where L is the room length; and U is the inlet velocity. Comparison of a vertical slice through the two simulations at $\tau = 100$ shows the two simulations produce very similar pollutant distributions (Figure 20), and time decay of

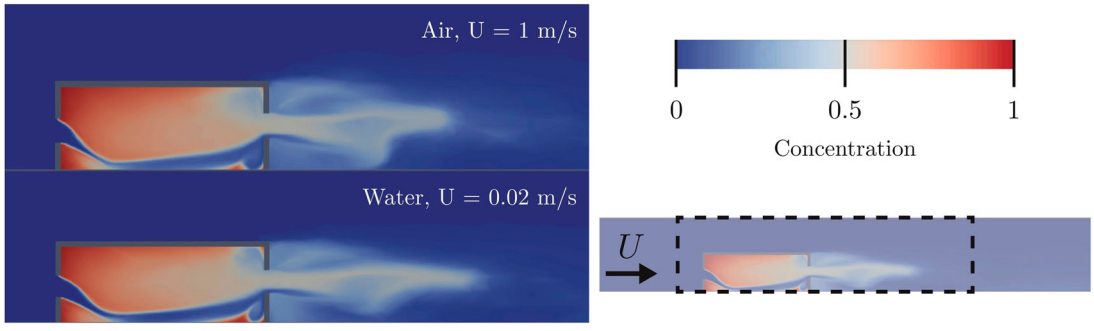

Figure 20. Comparison between full- and laboratory-scale simulations at $\tau = 100$. The room is initially full of pollutant (red), which is removed by cross-ventilation.

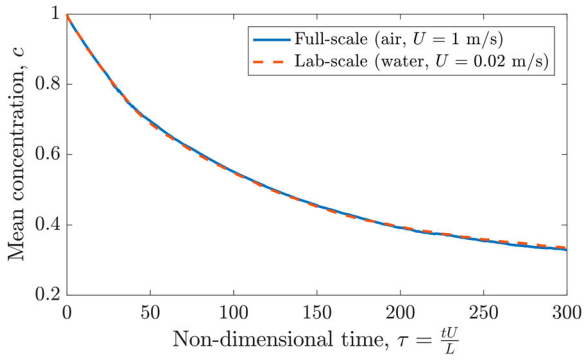

Figure 21. Decay of mean pollutant concentration with dimensionless time.

mean concentrations are in even better agreement (Figure 21). These preliminary simulations suggest that the dynamics that control the overall ventilation rates are not significantly affected by the reduction in Reynolds number, although further simulations are needed to confirm this finding, as identifying the true Reynolds number of an LES simulation is a complex issue.

Water flume experiments will examine the effect of temperature variations on a cross-ventilated room. The results of these experiments will be used to build simple theoretical descriptions that can be integrated into EnergyPlus, improving the modelling of internal flows and indoor–outdoor exchange.

Conclusions and future work

This paper reports research from the MAGIC project that aims to provide the tools to enable increased uptake of natural ventilation of buildings in cities, thereby reducing the urban heat island, building energy usage and GHG emissions. The research team has successfully carried out a field experiment and developed wind tunnel and Fluidity site models for flow and dispersion. Using these results, it is possible to create connections between internal conditions within the naturally ventilated building and the external environment. The connection between external and internal conditions is achieved by an interdisciplinary approach that uses wind tunnel-derived pressure coefficients and velocity data to test Fluidity predictions, and to provide input for building energy modelling such as EnergyPlus. It was shown that Fluidity can model interior flows and it was verified that small-scale water tank modelling can be used to obtain quantitative information even at reduced Reynolds numbers. The importance of roof shape was demonstrated by both Fluidity and wind tunnel simulations as well as some of the effects of traffic movement by Fluidity modelling. Precise control of air and surface temperatures in the wind tunnel will facilitate simulation of urban thermal phenomena such as dispersion under stable or unstable atmospheric conditions, the effects of differential solar irradiation, and the urban heat island.

ROMs and data assimilation are being developed by the authors to provide an optimized fast model for real-time operational use and to inform on the optimal location and operation of sensors. The capabilities of Fluidity will be improved through data assimilation and by including additional physical processes such as the effects of green and blue spaces. The accuracy of the representation of the outdoor environmental conditions (such as wind pressure coefficients) will be increased with further cross-validation of wind tunnel and Fluidity models, such that the indoor–outdoor exchanges can be sufficiently resolved to assess natural ventilation potential. This will also involve improved representation of indoor conditions (temperature and CO_2 variations in space and time) and improved modelling of the indoor–outdoor exchange.

The next step will be to integrate these components into a comprehensive tool to provide accurate predictions for a set of scenarios of interest to urban planners and architects. The next phase of the MAGIC project will examine more scenarios with naturally ventilated buildings within different local climate zones (different land-use cover and pollution levels). Future scenarios will help to identify the benefits of pedestrianizing a street (accounting for the displaced traffic) to understand how this process would be improved by the introduction of green or blue infrastructure (*e.g.* trees, fountains) and to identify beneficial changes to building design and operation with relevance to occupant wellbeing and the sustainability of urban communities.

Acknowledgements

The authors are very grateful to London South Bank University and the occupants of room DC222 for allowing them to install the monitors. The authors are also grateful to Southwark Council and Transport for London for their permission and assistance in placing the outdoor monitors.

Disclosure statement

No potential conflict of interest was reported by the authors.

Funding

This work was supported by the Engineering and Physical Sciences Research Council (EPSRC) Grand Challenge grant 'Managing Air for Green Inner Cities (MAGIC) [grant number EP/N010221/1].

ORCID

J. Song http://orcid.org/0000-0002-9483-0501
W. Lin http://orcid.org/0000-0002-2477-3521
L. Mottet https://orcid.org/0000-0002-0381-7521
M. Davies Wykes https://orcid.org/0000-0003-0316-0432
R. Arcucci http://orcid.org/0000-0002-9471-0585
D. Xiao http://orcid.org/0000-0003-2461-523X
P. F. Linden http://orcid.org/0000-0002-8511-2241

References

Andersson, E., Haseler, J., Unden, P., Courtier, P., Kelly, G., Vasiljevic, D., … Viterbo, P. (1998). The ECMWF implementation of three dimensional variational assimilation (3DVar). Part III: Experimental results. *Quarterly Journal of the Royal Meteorological Society*, *124*(550), 1831–1860. doi:10.1002/qj.49712455004

Aristodemou, E., Bentham, T., Pain, C., & Robins, A. (2009). A comparison of mesh-adaptive LES with wind tunnel data for flow past buildings: Mean flows and velocity fluctuations. *Atmospheric Environment*, *43*, 6238–6253. doi:10.1016/j.atmosenv.2009.07.014

Aristodemou, E., Boganegra, L. M., Mottet, L., Pavlidis, D., Constantinou, A., Pain, C., … ApSimon, H. (2018). How tall buildings affect turbulent air flows and dispersion of pollution within a neighbourhood. *Environmental Pollution*, *233*, 782–796. doi:10.1016/j.envpol.2017.10.041

Arnold, S. J., ApSimon, H., Barlow, J., Belcher, S., Bell, M., Boddy, J. W., … Walsh, P. (2004). Introduction to the DAPPLE Air Pollution Project. *Science of The Total Environment*, *332*, 139–153. doi:10.1016/j.scitotenv.2004.04.020

Badas, M. G., Ferrari, S., Garau, M., & Querzoli, G. (2017). On the effect of gable roof on natural ventilation in two-dimensional urban canyons. *Journal of Wind Engineering and Industrial Aerodynamics*, *162*, 24–34. doi:10.1016/j.jweia.2017.01.006

Baker, D. M., Huang, W., Guo, Y. R., Bourgeois, J., & Xiao, Q. N. (2004). A three-dimensional variational data assimilation system for MM5: Implementation and initial results. *Monthly Weather Review*, *132*, 897–914. doi:10.1175/1520-0493(2004)132

Baniassadi, A., & Sailor, D. J. (2018). Synergies and trade-offs between energy efficiency and resiliency to extreme heat – A case study. *Building and Environment*. doi:10.1016/j.buildenv.2017.01.037

Brixey, L. A., Heist, D. K., Richmond-Bryant, J., Bowker, G. E., Perry, S. G., & Wiener, R. W. (2009). The effect of a tall tower on flow and dispersion through a model urban neighbourhood; Part 2. pollutant dispersion. *Journal of Environmental Monitoring*, *11*, 2171–2179. doi:10.1039/b907137g

Brown, M. J., Lawson, R. E., DeCroix, D. S., & Lee, R. L. (2000). Mean flow and turbulence measurements around a 2-D array of buildings in a wind tunnel. In Proceedings of the 11th Joint AMS/AWMA Conference on the Applications of Air Pollution Meteorology. Long Beach, CA.

Cacuci, D. G., Navon, I. M., & Ionescu-Bujor, M. (2013). *Computational methods for data evaluation and assimilation*. London: Chapman and Hall/CRC.

Carpentieri, M., Hayden, P., & Robins, A. G. (2012). Wind tunnel measurements of pollutant turbulent fluxes in urban intersections. *Atmospheric Environment*, *46*, 669–674. doi:10.1016/j.atmosenv.2011.09.083

Daish, N. C., da Graça G., C., Linden, P. F., & Banks, D. (2016). Impact of aperture separation on wind-driven single-sided natural ventilation. *Building and Environment*, *108*, 122–134. doi:10.1016/j.buildenv.2016.08.015

Durst, F., Melling, A., & Whitelaw, J. H. (1976). *Principles and practice of laser-Doppler anemometry* (p. 410). London: Academic Press.

Fackrell, J. E., & Robins, A. G. (1982). Concentration fluctuations and fluxes in plumes from point sources in a turbulent boundary layer. *Journal of Fluid Mechanics*, *117*, 1–26. doi:10.1017/S0022112082001499

Ford, R., Pain, C. C., Piggott, M. D., Goddard, A. J. H., de Oliveira, C. R. E., & Umpleby, A. P. (2004). A nonhydrostatic finite-element model for three-dimensional stratified oceanic flows. Part I: Model formulation. *Monthly Weather Review*, *132*, 2816–2831. doi:10.1175/MWR2824.1

Garcia, X., Pavlidis, D., Gorman, G. J., Gomes, J. L. M. A., Piggott, M. D., Aristodemou, E., … ApSimon, H. (2011). A two-phase adaptive finite element method for solid-fluid coupling in complex geometries. *International Journal for Numerical Methods in Fluids*, *66*, 82–96. doi:10.1002/fld.2249

Ghiaus, C., Allard, F., Santamouris, M., Georgakis, C., & Nicol, F. (2006). Urban environment influence on natural ventilation potential. *Building and Environment*, *41*, 395–406. doi:10.1016/j.buildenv.2005.02.003

Grimmond, S. (2007). Urbanization and global environmental change: Local effects of urban warming. *Geographical Journal*, *173*(1), 83–88.

Heist, D. K., Brixey, L. A., Richmond-Bryant, J., Bowker, G. E., Perry, S. G., & Wiener, R. W. (2009). The effect of a tall tower on flow and dispersion through a model urban neighbourhood; Part 1. Flow characteristics. *Journal of Environmental Monitoring*, *11*, 2163–2170. doi:10.1039/b907135k

Kalnay, E. (2003). *Atmospheric modeling, data assimilation and predictability*. Cambridge: Cambridge University Press.

Linden, P. F. (1999). The fluid mechanics of natural ventilation. *Annual Review of Fluid Mechanics*, *31*, 201–238. doi:10.1146/annurev.fluid.31.1.201

Lorenz, E. N. (1956). *Empirical orthogonal functions and statistical weather prediction* (Sci. Rep. No. 1). Statistical Forecasting Project, Cambridge, MA: MIT.

Martins, N. R., & Carrilho da Graça, G. (2017). Impact of outdoor PM2.5 on natural ventilation usability in California's nondomestic buildings. *Applied Energy*, *189*, 711–724. doi:10.1016/j.apenergy.2016.12.103

Mateus, N., & Carrilho da Graça, G. (2015). A validated three-node model for displacement ventilation. *Building and Environment*, *84*, 50–59. doi:10.1016/j.buildenv.2014.10.029

Mead, M. I., Popoola, O. A. M., Stewart, G. B., Landshoff, P., Calleja, M., Hayes, M., … Jones, R. L. (2013). The use of electrochemical sensors for monitoring urban air quality in low-cost, high-density networks. *Atmospheric Environment*, *70*, 186–203. doi:10.1016/j.atmosenv.2012.11.060

Oke, T. R. (1973). City size and the urban heat island. *Atmospheric Environment*, *7*, 769–779. doi:10.1016/0004-6981(73)90140-6

Ordnance Survey. (2014). OS MasterMap® Building Heights [FileGeoDatabase geospatial data], Scale 1:2500, Tiles: tq37nw, tq38sw, Updated: 29 November 2014, Ordnance Survey (GB), Using: EDINA Digimap Ordnance Survey Service. Retrieved from http://digimap.edina.ac.uk

Ordnance Survey. (2016). OS VectorMap® Local [TIFF geospatial data], Scale 1:10000, Tiles: tq37nw, tq38sw, Updated: 23 September 2016, Ordnance Survey (GB), Using: EDINA Digimap Ordnance Survey Service. Retrieved from http://digimap.edina.ac.uk

Pain, C., Umpleby, A., De Oliveira, C., & Goddard, A. (2001). Tetrahedral mesh optimisation and adaptivity for steady-state and transient finite element calculations. *Computer Methods in Applied Mechanics and Engineering*, *190*, 3771–3796. doi:10.1016/S0045-7825(00)00294-2

Pavlidis, D., Gorman, G., Gomes, J., Pain, C., & ApSimon, H. (2010). Synthetic-Eddy method for urban atmospheric flow modelling. *Boundary-Layer Meteorology*, *136*, 285–299. doi:10.1007/s10546-010-9508-x

Sailor, D. J. (2001). Relating residential and commercial sector electricity loads to climate-evaluating state level sensitivities and vulnerabilities. *Energy*, *26*, 645–657. doi:10.1016/S0360-5442(01)00023-8

Sailor, D. J., & Pavlova, A. A. (2003). Air conditioning market saturation and long-term response of residential cooling energy demand to climate change. *Energy*, *28*, 941–951. doi:10.1016/S0360-5442(03)00033-1

Santamouris, M., Cartalis, C., Synnefa, A., & Kolokotsa, D. (2015). On the impact of urban heat island and global warming on the power demand and electricity consumption of buildings – A review. *Energy and Buildings*, *98*, 119–124. doi:10.1016/j.enbuild.2014.09.052

Santamouris, M., Papanikolaou, N., Livada, I., Koronakis, I., Georgakis, C., Argiriou, A., & Assimakopoulos, D. N. (2001). On the impact of urban climate on the energy consumption of buildings. *Solar Energy*, *70*(3), 201–216. doi:10.1016/S0038-092X(00)00095-5

Stewart, I. D., & Oke, T. R. (2012). Local climate zones for urban temperature studies. *Bulletin of the American Meteorological Society*, *93*(12), 1879–1900. doi:10.1175/BAMS-D-11-00019.1

UN-Habitat. (2011). *Cities and climate change: Global report on human settlements 2011*. London: Earthscan.

United Nations (UN). (2014). *The world urbanization prospects. The 2014 revision*. New York: United Nations, Department of Economic and Social Affairs, United Nations Publications.

Wang, Z., Xiao, D., Fang, F., Govindan, R., Pain, C., & Guo, Y. (2018). Model identification of reduced order fluid dynamics systems using deep learning. *International Journal for Numerical Methods in Fluids*, *86*(4), 255–268.

Wilby, R. L. (2003). Past and projected trends in London's urban heat island. *Weather*, *58*, 251–259. doi:10.1256/wea.183.02

Wood, C., Arnold, S. J., Balogan, A. A., Barlow, J. F., Belcher, S. E., Britter, R. E., … White, I. R. (2009). Dispersion experiments in central London; the 2007 Dapple project. *Bulletin of the American Meteorological Society*, *90*, 955–969. doi:10.1175/2009BAMS2638.1

Xiao, D., Fang, F., Buchan, A. G., Pain, C. C., Navon, I. M., Du, J., & Hu, G. (2014). Non-linear model reduction for the Navier–Stokes equations using residual DEIM. *Journal of Computational Physics*, *263*, 1–18. doi:10.1016/j.jcp.2014.01.011

Xiao, D., Fang, F., Pain, C. C., & Navon, I. M. (2017). A parameterized non-intrusive reduced order model and error analysis for general time-dependent nonlinear partial differential equations and its applications. *Computer Methods in Applied Mechanics and Engineering*, *317*, 868–889. doi:10.1016/j.cma.2016.12.033

Yassin, M. F. (2011). Impact of height and shape of building roof on air quality in urban street canyons. *Atmospheric Environment*, *45*(29), 5220–5229. doi:10.1016/j.atmosenv.2011.05.060